Supporting Information

Dinesh et al. 10.1073/pnas.1424077112

SI Experimental Procedures

Protein Expression and Purification. The pQE vector supporting expression of C-terminally $(His)_6$-tagged PsIAA4 DIII/IV (amino acid residues 86–189, 12.5 kDa) was described and mobilized into *Escherichia coli* strain M15[pREP] (Qiagen) (1). For unlabeled protein preparations, transformed cells were grown in double yeast extract trypton (2YT) medium containing 50 μg/mL ampicillin and 25 μg/mL kanamycin. Uniformly ^{15}N- or ^{13}C,^{15}N-labeled proteins were prepared by growing the bacteria in M9 medium supplemented with 1 g/L $^{15}NH_4Cl$ or 1 g/L $^{15}NH_4Cl$ and 2 g/L [^{13}C]glucose. Cells were grown at 37 °C to A_{600} = ∼0.8, and proteins were expressed in the presence of 1 mM isopropyl β-D-thiogalactopyranoside for 8 h at 37 °C or overnight at 18 °C. The bacterial pellets of 2-L cultures were resuspended in 50 mL of ice-cold buffer A (50 mM NaH_2PO_4, 300 mM $NaCl_2$, 2 mM $MgCl_2$, 20 mM imidazole, pH 7; for wild-type protein) or buffer B (50 mM HEPES–NaOH, 300 mM $NaCl_2$, 20 mM imidazole, pH 8; for mutant protein), each supplemented with 500 μL of Protease Inhibitor Mixture solution (Sigma P2714) and 1 mg/mL lysozyme. After incubation for 1–2 h, cell lysis was performed either by two passes through a French pressure cell or sonication, followed by incubation for 1–2 h with 20 μL of DNase I (2 mg/mL). The extracts were cleared by centrifugation at 20,000 × *g* for 30 min at 4 °C. The supernatants (50 mL) were loaded onto manually packed or prepacked 5 mL Co^{2+}-TALON resin columns (Clontech TALON Superflow/GE HiTrap-TALON crude). Columns were extensively washed with buffer A containing 100 mM imidazole for removing impurities. Proteins were eluted with buffer A containing 500 mM imidazole. Sample purity was verified by SDS/PAGE, and protein concentration was quantified by UV spectroscopy. Because purified wild-type PsIAA4 DIII/IV preparations formed homo-oligomers precluding NMR analysis, eluted wild-type protein samples were dialyzed overnight against buffer C (50 mM NaH_2PO_4, 2 mM $MgCl_2$, 5 mM DTT, 1 mM NaN_3, pH 2.5), which prevented protein aggregation, or against buffer D [50 mM Na-citrate buffer, 150 mM $NaCl_2$, 2 mM $MgCl_2$, 3 mM Tris-(2-chloroxyethyl)-phosphine hydrochloride, pH 6.25] for double- and triple-mutant protein preparations.

Mutagenesis. Site-directed mutagenesis was achieved with the QuikChange Site-Directed Mutagenesis Kit (Agilent Technologies). All plasmids were verified by DNA sequencing.

Analytical Ultracentrifugation. Analyses of PsIAA4 DIII/IV preparations were performed by using a Beckman XL-A centrifuge (Beckman Coulter), an An50Ti rotor, and double sector cells. Sedimentation equilibria were monitored at 14,000 rpm and 20 °C (A_{280}). Sedimentation velocities were analyzed by taking scans every 10 min at 40,000 rpm and 20 °C (A_{230} or A_{280}). Data analysis was conducted by using Sedfit (2).

ITC. ITC studies were performed on a MicroCal iTC200 microcalorimeter (Malvern). Both mutant proteins, PsIAA4 $PB1^{AM3}$ and $PB1^{BM3}$, were dialyzed for 8–12 h against the buffer (50 mM Na-citrate, 300 mM NaCl, 2 mM $MgCl_2$, and 1 mM TCEP, pH 6.25). After thermal equilibrium at 25 °C and initial injection (0.4 μL) of the titrant ($PB1^{BM3}$), 20 injections (2 μL) of $PB1^{BM3}$ (960 μM) were added to the stirred sample cell (200 μL) containing $PB1^{AM3}$ (96 μM) at intervals of 150 or 240 s to achieve a final complete binding isotherm. The heat associated with each titration peak was integrated and plotted against the respective molar ratio of two mutant proteins. The titrant's heat of dilution was calculated from the last few injections after saturation and subtracted to obtain effective heats of binding. Data were analyzed by using nonlinear least-squares curve fitting using the standard one-binding site model supplied with Origin (Version 7.0; OriginLab Corp.). Thermodynamic parameters of dimer formation were also measured at different temperatures (15–35 °C) with $PB1^{BM3}$ (700 μM) and $PB1^{AM3}$ (70 μM) using the same experimental conditions.

Y2H Assays. The full-length PsIAA4 coding sequence (3) was amplified by using Gateway-cloning compatible primers and Gateway Technology. Purified PCR products were mobilized into pDONR221 entry vector via the BP clonase recombination reaction. Point mutations were introduced by site-directed mutagenesis as described above. The constructs for LexA Y2H assays were generated via LR clonase recombination reactions from the respective entry clones and mobilized into Gateway-compatible versions of pGlida (for DBD hybrids) and pB42AD (for AD hybrids) vectors. DBD and AD constructs were transformed into *Saccharomyces cerevisiae* strains EGY48 (MATα) carrying the LacZ reporter plasmid pSH18-34 and YM4271 (MATa), respectively. After mating, diploids were selected on SD/-Ura/-His/-Trp and assessed for activation of the β-galactosidase reporter gene on Gal/Raf/-Ura/-His/-Trp medium supplemented with X-Gal as described (4). Expression of PsIAA4 fusion proteins was analyzed by preparing crude total protein extracts from diploid yeast followed by SDS/PAGE and immunoblotting using antibodies against HA-tag (Santa Cruz Biotechnology; sc-7392; detection of AD-hybrids) or LexA (Abcam ab14553; detection of DBD-hybrids) followed by incubation with HRP-conjugated anti-mouse (Thermo Scientific no. 31430) and anti-rabbit (Santa Cruz Biotechnology; no. sc-2004) secondary antibodies, respectively. Protein bands were detected by using the SuperSignal West Pico Chemiluminescent Kit (Thermo Scientific) and imaged (AlphaInnotech FluorChem Q).

Data-Driven Protein–Protein Docking. The HADDOCK Easy interface (haddock.science.uu.nl/services/HADDOCK) was used to initiate directional docking with two monomer structures as input. Defined active residues derived from experiments (NMR and Y2H assays) were specified, and passive surrounding surface residues were selected automatically. Data were converted in highly ambiguous intermolecular restraints to drive docking with the PsIAA4 PB1 monomer ensemble (10 lowest energy structures) to allow more flexibility. Docking resulted in 11 clusters of 164 structures, which represent 82% of the water-refined models generated. The top 10 clusters with lowest Z-scores were used for selecting the four best structures of each cluster for detailed analysis of PsIAA4 PB1 homodimer models by PDBsum Generate (5).

1. Colón-Carmona A, Chen DL, Yeh KC, Abel S (2000) Aux/IAA proteins are phosphorylated by phytochrome in vitro. *Plant Physiol* 124(4):1728–1738.
2. Schuck P (2000) Size-distribution analysis of macromolecules by sedimentation velocity ultracentrifugation and lamm equation modeling. *Biophys J* 78(3):1606–1619.
3. Kim J, Harter K, Theologis A (1997) Protein-protein interactions among the Aux/IAA proteins. *Proc Natl Acad Sci USA* 94(22):11786–11791.
4. Calderón Villalobos LI, et al. (2012) A combinatorial TIR1/AFB-Aux/IAA co-receptor system for differential sensing of auxin. *Nat Chem Biol* 8(5):477–485.
5. Laskowski RA, et al. (1997) PDBsum: A Web-based database of summaries and analyses of all PDB structures. *Trends Biochem Sci* 22(12):488–490.

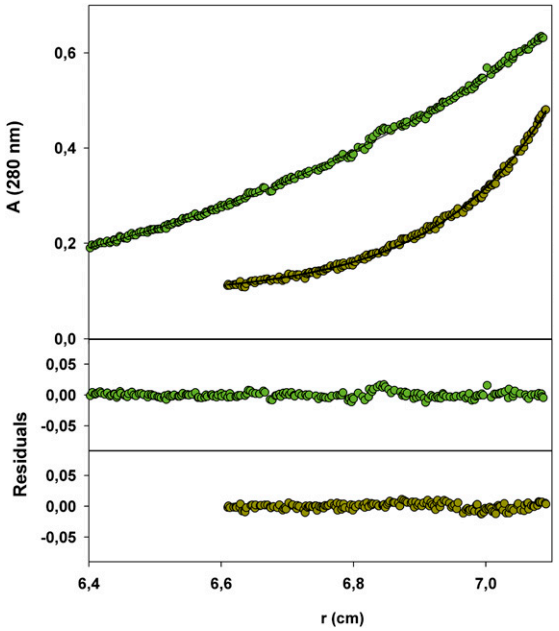

Fig. S1. Average molecular mass determination of wild-type PsIAA4 DIII/DIV by sedimentation equilibrium. Analytical ultracentrifugation studies of purified wild-type PsIAA4 DIII/IV protein were carried out at 20 °C, and data were collected at a rotor speed of 14,000 rpm (see *Experimental Procedures*). *Upper* shows the experimental data, and *Lower* shows the residuals. PsIAA4 DIII/DIV exists as a monomeric species (15 kDa) at pH 3.0 (green), whereas oligomeric species (45 kDa) dominate at pH 8.0 (olive). The apparent molecular masses were calculated as described in *Experimental Procedures*.

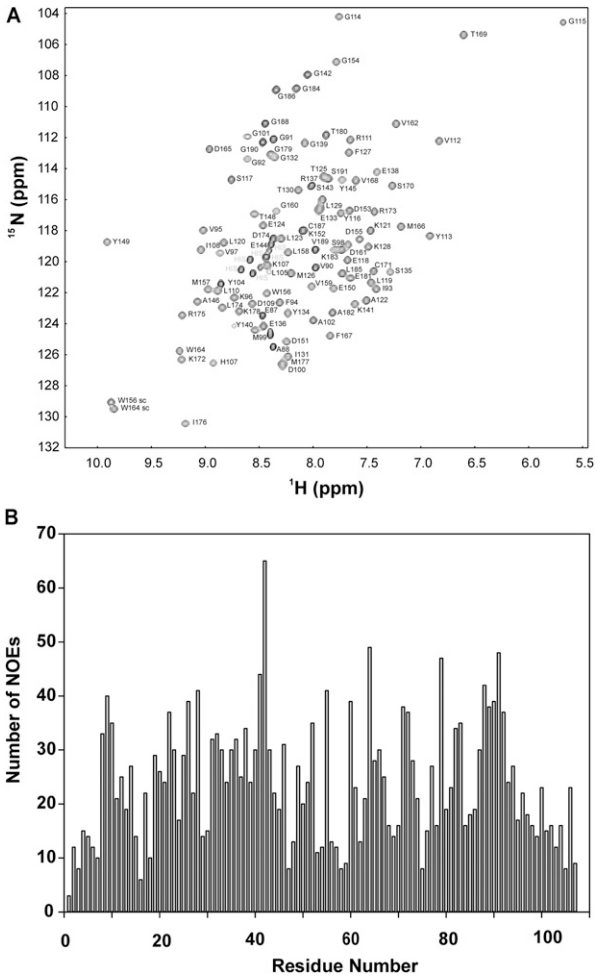

Fig. S2. Backbone assignment of PsIAA4 DIII/IV and transient NOEs. (*A*) The ^{1}H-^{15}N HSQC spectrum of wild-type PsIAA4 DIII/IV was measured at 800 MHz, 25 °C, and pH 2.5. Each cross-peak corresponding to the backbone chemical shift information of an individual amino acid residue is labeled by the one-letter code of amino acids followed by residue number. Sequential backbone assignment was performed with a standard set of 3D NMR experiments using NMRview. His-tag residues were labeled in gray. (*B*) Bar diagram showing the number of transient NOE contacts of each PsIAA4 DIII/IV residue indicate high data quality, which was used for subsequent NMR structure calculation.

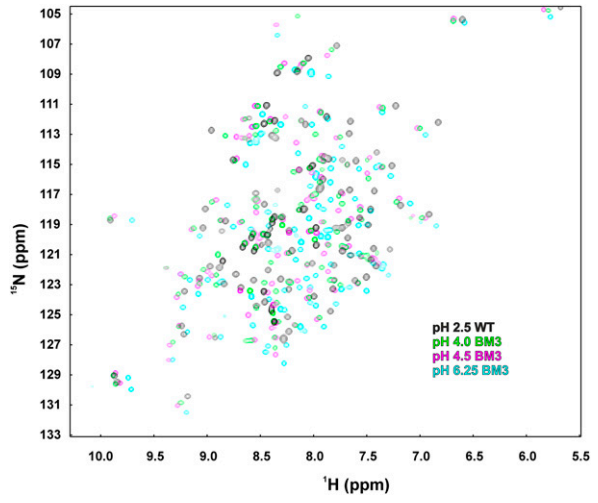

Fig. S3. NMR-based pH scanning of PsIAA4 PB1^{BM3} protein. Overlay of ^{1}H-^{15}N HSQC spectra of wild-type PsIAA4 PB1 at pH 2.5 (black) and mutant PsIAA4 PB1^{BM3} recorded at pH 4.0 (green), pH 4.5 (magenta), and pH 6.25 (cyan). The data were used for sequential backbone assignment of PsIAA4 PB1^{BM3}.

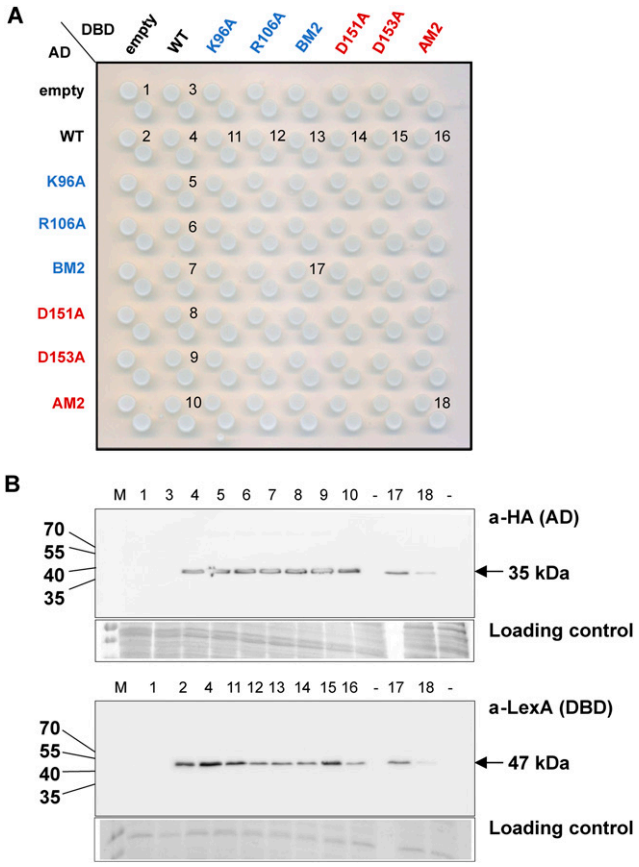

Fig. S4. Controls for Y2H assays of homotypic PsIAA4 interaction. (*A*) Growth controls of PsIAA4 diploids on selective medium (SD/-Ura/-His/-Trp). Diploids were spotted as in Fig. 4*A*. (*B*) Immunoblot analysis revealed that PsIAA4 protein variants accumulate in all selected diploids. α-HA (for HA-tagged AD hybrids) and α-LexA (for DBD hybrids) antibodies were used on immunoblots of extracts prepared from diploids expressing PsIAA4 wild type and variants as labeled in *A*. Silver-stained nonspecific bands of yeast total protein extracts are shown as loading control.

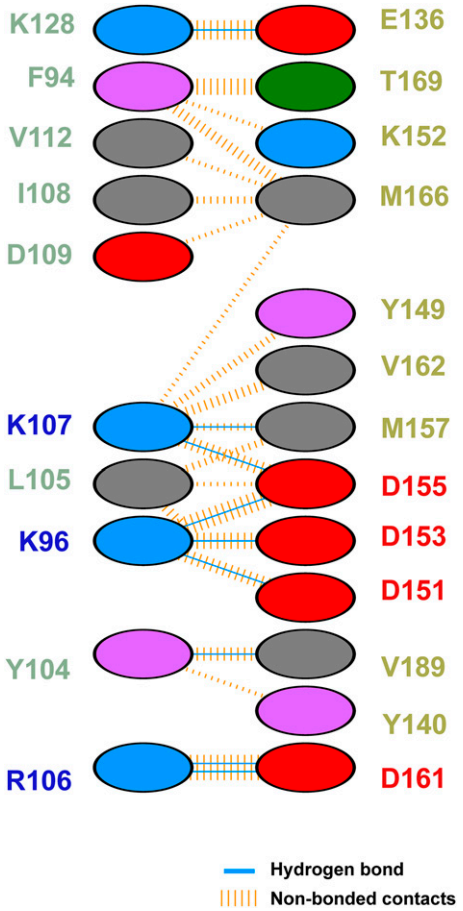

Fig. S5. Protein–protein interface analysis of the PsIAA4 PB1 homodimer model. The final HADDOCK PsIAA4 PB1 homodimer model was analyzed by using PDBsum Generate, which was used to display additional interface residues and their interactions (hydrogen bonds and nonbonded contacts). These are depicted in a cartoon diagram together with the basic (K96, R106, and K107) and acidic (D151, D153, D155, and D161) amino acid residues of the canonical PB1 features. The thickness of nonbonded contacts is proportional to the number of atomic contacts.

Structure (method)	Chain	No. of residues	Area (Å^2)	Salt-bridges	S-S	H-bonds	Non-bonded contacts
PsIAA4 PB1 (NMR and HADDOCK)	A B	10 13	698 644	-	-	9	~ 70
ARF5 PB1 (X-ray)	D B	14 11	567 630	-	-	12	81

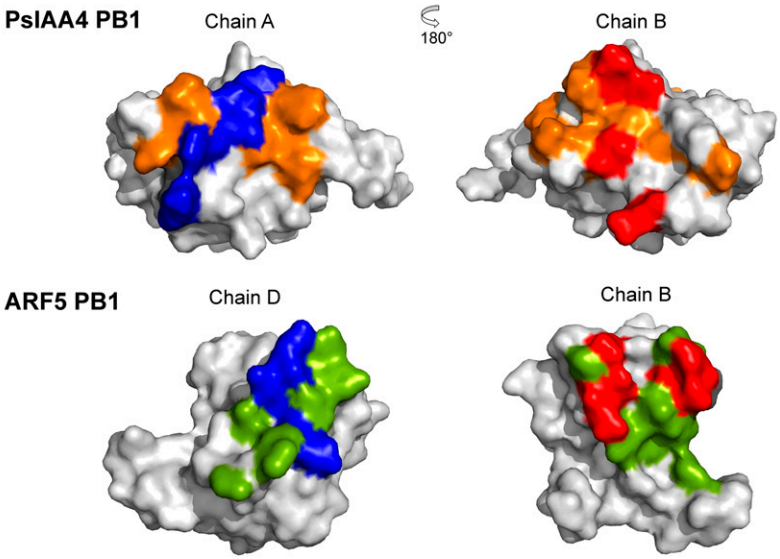

Fig. S6. Interaction surfaces of the PsIAA4 and ARF5 PB1 homodimer. The table lists interface statistics for PsIAA4 PB1 (this study) and ARF5 PB1 (1). Complementary interaction faces of the two monomers (chains A and B) are shown below for each PB1 domains. Basic and acidic surface residues interacting via hydrogen bonds are labeled in blue and red, respectively. Hydrophobic and polar residues engaging on nonbonded contacts are labeled in orange (PsIAA4 PB1) or green (ARF5 PB1).

1. Nanao MH, et al. (2014) Structural basis for oligomerization of auxin transcriptional regulators. *Nat Commun* 5:3617–3624.

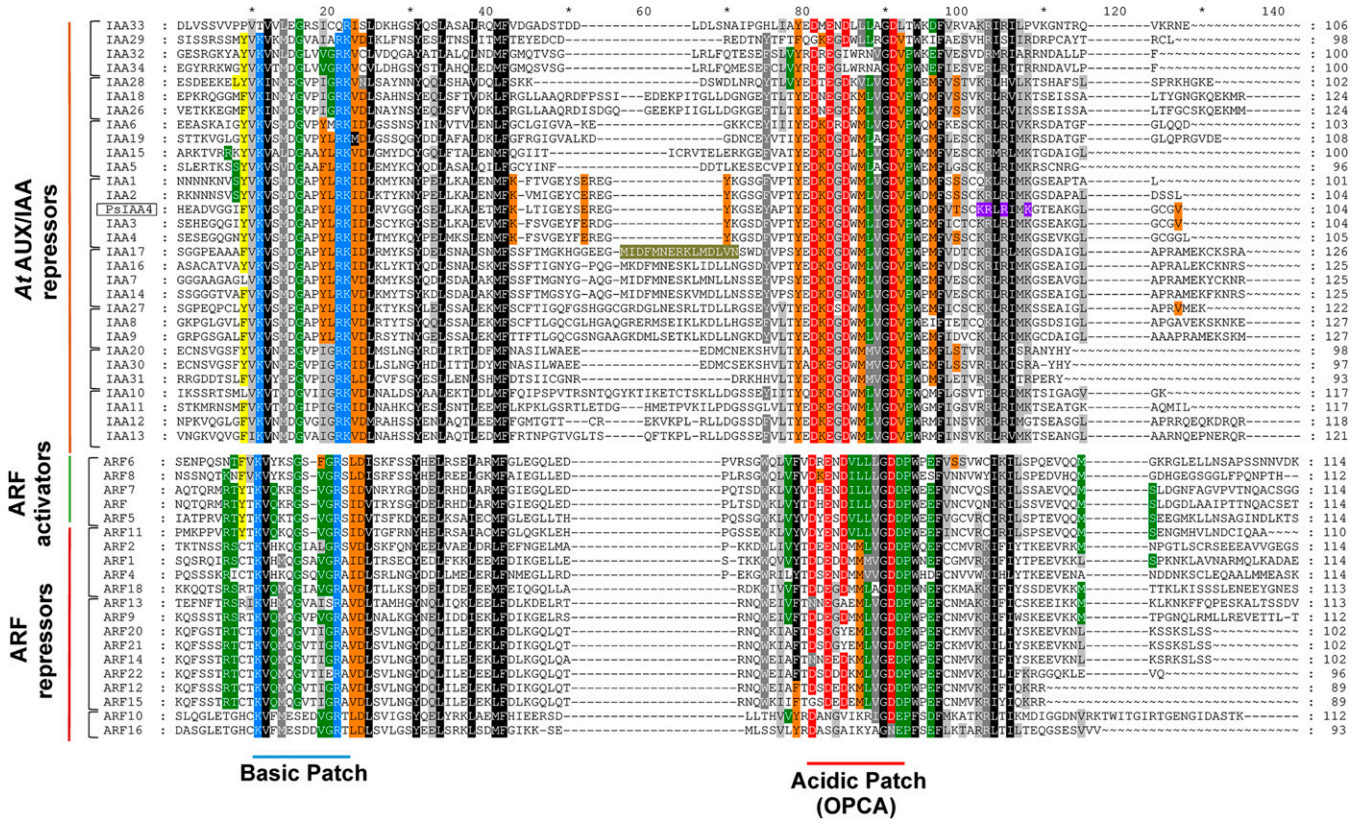

Fig. S7. Multiple sequence alignment of the PB1 domains of PsIAA4 and *Arabidopsis* AUX/IAA and ARF families. The canonical features of type I/II PB1, the invariant Lys residue and OPCA motif, are highlighted in blue (basic patch) and red (acidic patch), respectively. Residues of the homodimeric interface of PsIAA4 PB1 (HADDOCK generated) and ARF5 PB1 (X-ray structure) that are conserved or frequently occur in both families are indicated in orange and green, respectively. The aromatic interface residue common to both groups is highlighted in yellow. The insertion helix α1′ of IAA17 (1) is highlighted in olive green. If not part of the interaction interface, other conserved positions in both families are highlighted in gray shades.

1. Han M, et al. (2014) Structural basis for the auxin-induced transcriptional regulation by Aux/IAA17. *Proc Natl Acad Sci USA* 111(52):18613–18618.

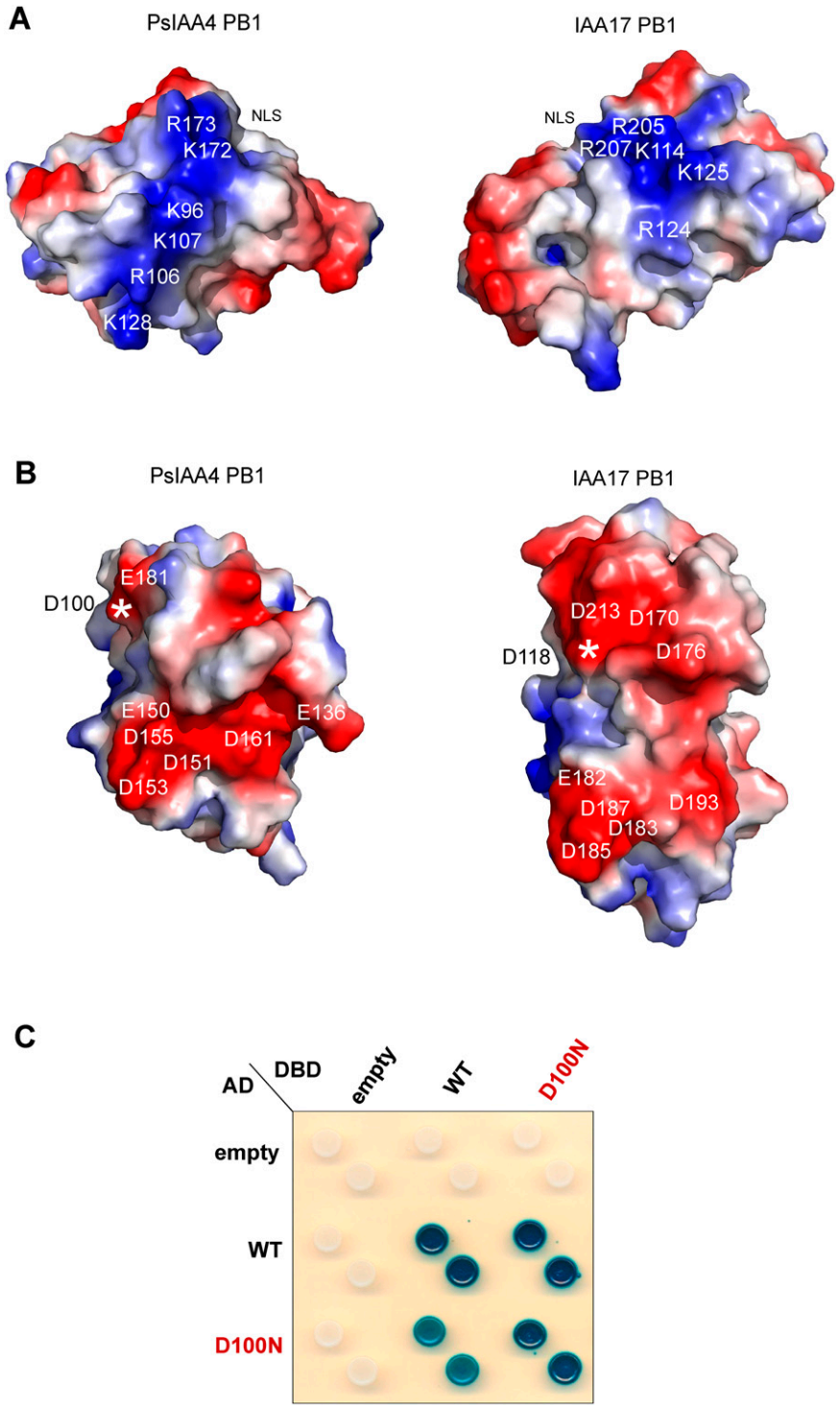

Fig. S8. Comparison of PsIAA4 and *Arabidopsis* IAA17 PB1 domain surface electrostatics. (*A* and *B*) Overall electrostatic surface charges of the basic (*A*) and acidic (*B*) surface patches of PsIAA4 and IAA17 PB1 domains. Note that wild-type amino acid residues were reintroduced in silico into the NMR structure of the mutant IAA17 PB1 domain (1). Amino acid residues K172/R173 (PsIAA4 PB1) and R205/R207 (IAA17 PB1) are part of the NLS conserved in AUX/IAA proteins. The amino acid residues D118/D213, together with helix α3 (D170/D176), extend the acidic OPCA surface on IAA17 PB1. The D118N mutation (asterisk) prevents homodimerization and heterodimerization of IAA17 in yeast (2). (*C*) However, in PsIAA4 the corresponding acidic D100/E181 patch is separated from the OPCA motif, and the D100N mutation (asterisk) of full-length PsIAA4 does not disrupt homotypic interaction in the Y2H assay.

1. Han M, et al. (2014) Structural basis for the auxin-induced transcriptional regulation by Aux/IAA17. *Proc Natl Acad Sci USA* 111(52):18613–18618.
2. Ouellet F, Overvoorde PJ, Theologis A (2001) IAA17/AXR3: Biochemical insight into an auxin mutant phenotype. *Plant Cell* 13(4):829–841.

Table S1. NMR structure constraints and refinement statistics for wild-type PsIAA4 DIII/IV

NMR distance and dihedral constraints	
Distance constraints	1,927
Total unambiguous NOE	1,424
Intraresidue	606
Interresidue	
Sequential ($\|i - j\| = 1$)	351
Medium-range ($\|i - j\| < 4$)	187
Long-range ($\|i - j\| > 5$)	280
Total ambiguous NOE	503
Intermolecular	0
Hydrogen bonds	0
Total dihedral angle restraints	174
phi	87
psi	87
Structure statistics	
Violations (mean and SD)	
Distance constraints, Å	0.024 ± 0.001
Dihedral angle constraints, °	2.0 ± 0.1
Max. dihedral angle violation, °	6.0
Max. distance constraint violation, Å	2.1
Ramachandran analysis	
Most favored, %	86.1
Additionally allowed, %	11.7
Generously allowed, %	0.7
Disallowed, %	1.5
Deviations from idealized geometry	
Bond lengths, Å	0.001
Bond angles, °	0.32
Impropers, °	0.21
Average pairwise rmsd,* Å	
Heavy	0.98 ± 0.06
Backbone	0.66 ± 0.07

*Pairwise rmsd was calculated among 10 refined structures of PsIAA4DIII/IV (86–189) along with 3 additional residues (Gly-Ser-His) at its C terminus without the His-tag.

Table S2. Thermodynamic parameters of temperature-dependent dimer formation of PsIAA4 $PB1^{BM3}$ and PsIAA4 $PB1^{AM3}$

T, °C	ΔH, kcal/mol	ΔS, cal/mol per K	TΔS, kcal/mol	K_D, μM	ΔG, kcal/mol
15	−1.789	17.6	5.0688	6,2	−6.86
25	−2.815	14.3	4.2614	6,4	−7.07
35	−3.522	12.8	3.9424	5,1	−7.47